Unveiling Liquid-Phase Exfoliation of Graphite and Boron Nitride Using Fluorescent Dyes Through Combined Experiments and Simulations

Yilin He, Xuliang Qian, Guilherme Carneiro Queiroz da Silva, Cristian Paola Gabellini, Matteo Andrea Lucherelli, Giacomo Biagiotti, Barbara Richichi, Cécilia Ménard-Moyon, Huajian Gao, Paola Posocco, et al.

Unveiling liquid-phase exfoliation of graphite and boron nitride using fluorescent dyes through combined experiments and simulations

Yilin He, Xuliang Qian, Guilherme Carneiro Queiroz Da Silva, Cristian Gabellini, Matteo Andrea Lucherelli, Giacomo Biagiotti, Barbara Richichi,* Cécilia Ménard-Moyon, Huajian Gao,* Paola Posocco,* Alberto Bianco*

Yilin He, Dr. Matteo Andrea Lucherelli, Dr. Cécilia Ménard-Moyon, Dr. Alberto Bianco
CNRS, Immunology, Immunopathology and Therapeutic Chemistry, UPR 3572, University of Strasbourg, ISIS, 67000 Strasbourg, France. E-mail: a.bianco@ibmc-cnrs.unistra.fr

Dr. Xuliang Qian
School of Mechanical and Aerospace Engineering, Nanyang Technological University, 50 Nanyang Avenue, 639798 Singapore

Dr. Matteo Andrea Lucherelli
Instituto de Ciencia Molecular (ICMol), Universitat de Valencia, Carrer del Catedrátic José Beltrán Martinez, 2, 46980 Paterna, Valencia, Spain

Prof. Huajian Gao
School of Mechanical and Aerospace Engineering, Nanyang Technological University, 50 Nanyang Avenue, 639798 Singapore
Institute of High Performance Computing, A*STAR, 138632 Singapore. E-mail: huajian.gao@ntu.edu.sg

Dr. Guilherme Carneiro Queiroz Da Silva, Cristian Gabellini, Prof. Paola Posocco
Department of Engineering and Architecture, University of Trieste, 34127 Trieste, Italy. E-mail: PAOLA.POSOCCO@dia.units.it

Dr. Giacomo Biagiotti, Prof. Barbara Richichi
Department of Chemistry 'Ugo Schiff', University of Firenze, 50019 Sesto Fiorentino (Firenze) Italy. E-mail: barbara.richichi@unifi.it

Keywords: two-dimensional materials, sonication-assisted exfoliation, molecular self-assembly, adsorption

Liquid-phase exfoliation (LPE) in aqueous solutions provides a simple, scalable and green approach to produce two-dimensional (2D) materials. By combining atomistic simulations with exfoliation experiments, the interaction between a surfactant and a 2D layer at the molecular scale can be better understood. In this work, two different dyes, corresponding to rhodamine B base (Rbb) and to a phenylboronic acid BODIPY (PBA-BODIPY) derivative, are employed as dispersants to exfoliate graphene and hexagonal boron nitride (hBN) through sonication-assisted LPE. The exfoliated 2D sheets, mostly as few-layers, exhibit good quality and high loading of dyes. Using molecular dynamics (MD) simulations, the binding free energies are calculated and the arrangement of both dyes on the layers are predicted. We find that the dyes show a higher affinity towards hBN than graphene, which is consistent with the higher yields of exfoliated hBN. Furthermore, we demonstrate that the adsorption behavior of Rbb molecules on graphene and hBN is quite different compared to PBA-BODIPY.

1. Introduction

With the successful isolation of monolayered graphene from graphite, extensive researches and applications have emerged due to its extraordinary properties, such as an ultrathin planar structure, a high mechanical stiffness and strength, an excellent thermal and electrical conductivities and a good biocompatibility.[1,2] Since then, a series of other 2D materials with distinctive physical, chemical and electrical characteristics have been isolated, including hexagonal boron nitride (hBN),[3,4] transition metal carbides (MXenes),[5,6] transition metal dichalcogenides (TMDs),[7,8] and Xenes like black phosphorous (BP).[9,10] Among them, hBN is known as a structural analogue of graphene with alternative boron and nitrogen replacing carbon to form the 2D layered structure.[11] Unlike graphene with zero band gap, hBN possesses a wide band gap and partially ionic B–N bonds, as well as a host of optical, electrical and chemical properties with extensive applications in lubrication products, cosmetics, electronic devices and composites.[12,13] In order to fully exploit the morphological, chemical and physical advantages of 2D materials, it is crucial to produce them with controlled properties, high quality and dispersibility in green solvent. Top-down exfoliation and bottom-up synthesis are two main approaches to obtain layered materials, the former process permitting to produce materials at the industrial scale from naturally abundant bulk materials in a cheap and simple way.[14] Liquid-

phase exfoliation (LPE) has emerged as the most attractive method to produce 2D materials by overcoming the interlayer van der Waals force characteristics of the bulk materials.[15] This approach permits, using organic solvents, to obtain stable dispersions of single- and few-layer graphene and other materials.[16,17] However, the toxicity as well as high cost of organic solvents used in LPE have limited their applications. In contrast, the use of water in LPE provides an ideal environmental-friendly approach, opening also the opportunity of exploiting 2D materials for biological applications, such as cancer therapy, drug delivery, biosensing, bioimaging and antibacterial uses.[18-20]

However, LPE of bulk materials in pure water faces the problem of poor efficiency because of the hydrophobic nature of the materials. To solve this problem, exfoliating agents have been used as dispersants to improve the dispersibility and exfoliation yield.[21,22] These compounds can be divided into two main types: i) water-soluble small aromatic molecules and ii) surfactants. [15] Polycyclic aromatic hydrocarbons (PAH) are the typical aromatic molecules that resulted in efficient exfoliation.[23,24] For example, different types of pyrene derivatives can intercalate between the layers and adsorb through π–π interactions, leading to the high-yield exfoliation of graphene in water at basic pH.[23] Apart from small aromatic molecules, surfactants are amphiphilic molecules that have been investigated as surface stabilizers of 2D materials. The structure of surfactants contains a hydrophobic part, which can adsorb on the surface of a sheet and a hydrophilic head helping exfoliated flakes to remain dispersed in water.[25,26] Surfactant-assisted LPE in water also allows for new perspectives for biomedical applications. For instance, sodium cholate was employed to exfoliate and stabilize WS_2 sheets in water for antibacterial applications.[27] Alternatively, our group used sodium cholate to exfoliate hBN and investigated its interactions with the cell membrane, with result evidencing the formation of water channels leading to lysosomal membrane permeabilization.[28]

Fluorescent dyes have been widely applied in diagnosis, photodynamic therapy, and cell imaging.[29,30] Rhodamine and boron-dipyrromethene derivatives are two typical fluorescent dyes with high fluorescence quantum yield and excellent photostability.[31,32] Moreover, BODIPY derivatives and rhodamine dyes showed non-cytotoxic effects at low concentration.[33,34] Additionally, their similar aromatic central molecular core structure makes them promising candidates as dispersants to tightly adsorb onto flat materials through non-

covalent interactions. Here, we explore rhodamine and BODIPY dyes as potential molecules to improve the exfoliation of 2D materials in water and produce highly stable dispersions. For this purpose, graphite and bulk hBN were exfoliated in water with the assistance of rhodamine B base (Rbb) and a phenylboronic acid BODIPY (PBA-BODIPY) derivative (**Figure 1a**).[35] The structure of Rbb and PBA-BODIPY derivative includes aromatic groups and hydrophilic parts, facilitating non-covalent interactions with the sheets and ensuring stable dispersibility. The few-layer graphene and hBN were obtained with high quality and found to be well-dispersible in water at a concentration of 0.2 mg/mL with a good colloidal stability. Due to electron transfer, the fluorescence of the dyes was likely quenched after adsorption on graphene or hBN sheets. Both BODIPY and rhodamine have been employed in various strategies for biomedical applications. It has been reported that at low concentration (below 500 nM), BODIPY derivatives showed no cytotoxicity.[36] In another report, rhodamine complexes have been explored for MRI and fluorescence imaging.[37] A cytotoxicity study demonstrated good biocompatibility at concentrations up to 1 mM. As reported in several other studies, the loading of aromatic molecules onto graphene or hBN sheets is usually <10 % w/w,[28,38] corresponding to concentrations lower than 0.05 mM in 100 μg/mL of exfoliated nanosheets. Moreover, in our case the dye release was very low (*vide infra*), thus minimizing the risk of potential cytotoxic effects.

Thus, the fluorescence property of the exfoliated sheets was also investigated in view of their possible use in bioimaging. In addition, molecular simulations were performed to investigate the interaction between the layers of graphene and hBN and the two exfoliating dyes. The results contribute to a more comprehensive understanding of the exfoliation efficiency with aromatic dyes and may guide future design of fluorescent-exfoliating dispersants, to obtain in one step production biologically trackable 2D materials.

2. Experiment Section

2.1 Materials preparation

hBN was purchased from Alfa Aesar. Graphite powder was purchased from Sigma-Aldrich. The PBA-BODIPY was synthesized using a previously published protocol.[39] All other reagents were obtained from Sigma-Aldrich. hBN powder was ball milled with a Rescht Planetary Ball Mill

PM 100 for 20 h at 100 rpm at room temperature before exfoliation. Elma model Elmasonic P was used as water bath supersonic device for exfoliation. The temperature during bath sonication was kept at 20~30°C. Beckman Avant J-25 centrifuge was employed to centrifuge the materials after exfoliation. Omnipore® 0.1 μm PTFE membranes from Merck Millipore were used for filtration.

hBN was exfoliated in the presence of Rbb and PBA-BODIPY in water using ball milling and bath sonication. In detail, hBN (120 mg) and Rbb (120 mg) were ball milled for 3 h at 100 rpm. The mass ratio of m_{hBN}/m_{Rbb} is 1:1. Then, the mixed powder was recovered in 40 mL water, followed by bath sonication at 37 MHz for 6 h. After sonication, the dispersion was centrifuged at 500 g for 1 h to collect the supernatant. The supernatant was filtered and washed with 800 mL water. Then, the membrane filter was sonicated in 20 mL water and the dispersion was kept at 4°C overnight. After that, the most stable hBN-Rbb sheets were obtained by collecting the supernatant, discarding the new precipitated material. For the exfoliation of hBN with PBA-BODIPY, 30 mg hBN and 5 mg of PBA-BODIPY were dispersed in 1 mL water, followed by bath sonication for 30 min. The mass ratio of $m_{hBN}/ m_{PBA\text{-}BODIPY}$ is 6:1. After the dispersion was lyophilized to get a homogeneous powder, ball milling was carried out for 3 h at 100 rpm. The powder was recovered in 15 mL water, and 85 μL of *N,N*-diisopropylethylamine were added. The dispersion was sonicated for 5 h at 37 MHz and centrifuged at 402 g keeping the temperature at 10°C for 90 min. Then, the supernatant was filtered and washed using 100 mL water to remove the excess of PBA-BODIPY. The hBN-BODIPY sheets were recovered by sonication in 3 mL water as stock solution.

Graphite was exfoliated in the presence of Rbb and PBA-BODIPY in water using bath sonication. Graphite (1.5 g) and Rbb (200 mg) were dispersed in 200 mL water and sonicated for 5 h at 37 MHz. The mass ratio of $m_{graphite}/m_{Rbb}$ is 7.5:1. Then, the dispersion was centrifuged at 1500 g for 1 h, filtered and washed with 800 mL water. The exfoliated layers were recovered in 20 mL water by sonication for 5 min (sample named G-Rbb). Exfoliation of graphite with PBA-BODIPY was carried out in 3 mL MeOH/H_2O mixture (4:1). Graphite (100 mg) and 50 μL *N,N*-diisopropylethylamine were added into 1 mg/mL solution of PBA-BODIPY. The mass ratio of $m_{graphite}/m_{PBA\text{-}BODIPY}$ is 100:3. The solution was sonicated for 5 h at 37 MHz and centrifuged at 1500 g for 45 min. The supernatant containing exfoliated graphite sheets was

filtered and wash with 100 mL water. After these steps, the BODIPY-exfoliated graphene (named G-BODIPY) was collected by bath sonication in 10 mL water for 5 min.

One mL of dispersed graphene/hBN solution was filtered with 0.1 μm PTFE membranes, followed by drying under vacuum to weight the remaining solid and calculate the concentration of the stock dispersion.

2.2 Characterization of exfoliated graphene and hBN

Dynamic light scattering (DLS) and zeta potential measurements were performed on a Malvern Zetasizer Nano ZS (Malvern Instruments) at 25°C using a DTS1070 cell to obtain the hydrodynamic size and surface charge of the exfoliated sheets. The morphology and lateral size of the nanosheets were observed under a Hitachi 7500 transmission electron microscope (TEM). High resolution TEM was performed on a JEOL 2100F TEM electron microscope to assess the number of layers. Atomic Force Microscope analysis (AFM) measurements were conducted using a Bruker dimension ICON AFM, using the scan ScanAssist mode in air, using scan assist TAP300G. Images were obtained by scanning surfaces between 1 and 15 μm of lateral size and with 512 lines each. Graphene and hBN sheets were deposed by spin coating on SiO_2 substrates previously cleaned with water, isopropanol and base piranha solution. X-ray powder diffraction (XRD) patterns was performed by Bruker D8 X-ray diffractometer. Raman spectra were obtained on a Renishaw inVia microRaman with 532 nm laser under a Leica microscope. Thermogravimetric (TGA) analysis was performed on a TGA1 (Mettler Toledo) apparatus using platinum pans. The TGA temperature ranged from 40°C to 900°C with a ramp of 10°C/min under N_2 using a flow rate of 50 mL/min. The loading percentage of dispersants was calculated as:

$$Loading\ \ percentage = \frac{W_{EL} - W_{BL}}{W_{DL} - W_{BL}} \times 100\%$$

where W_{EL} is the weight loss of exfoliated materials at 900°C, W_{BL} the weight loss of bulk materials at 900°C and W_{DL} the weight loss of dispersants at 900°C.

X-ray photoelectron spectroscopy (XPS) was performed on a Thermo Scientific KAlpha X-ray photoelectron spectrometer. The samples were lyophilized and deposited onto a scotch tape (3MTM EMI Copper Foil Shielding Tape 118) with a spot size of 400 μm. The C 1s

photoelectron binding energy was set at 284.5 ± 0.2 eV and used as a reference for calibrating the other peak positions. The basic chamber pressure is 10^{-8}-10^{-9} bar and an Al anode was used as the X-ray source (1486 eV). The survey spectra were shown as an average of 10 scans with a pass energy of 200.00 eV and a step size of 1 eV. High-resolution spectra were displayed as an average of 20 scans with a pass energy of 50.00 eV and a step size of 0.1 eV. Each sample was repeated 3 times. UV-Vis absorption spectra were recorded on a Cary 5000 UV-Vis-NIR spectrophotometer and were corrected for the baseline using the solvent as blank. Fluorescence emission spectra were measured on a Fluorolog FL3-22 (Horiba Jobin Yvon) spectrometer using a swig xenon 450 W lamp, employing standard correction files, and recording the reference signal.

2.3 Computational methods

Graphene and hBN nanosheet models were prepared following a computational protocol published previously by part of the group.[28,40,41] Briefly, automated topology builder (ATB) [42-44] was employed to generate the topologies and parameters that were compatible with the GROMOS54a7 force field.[45] An empirical force field was adopted for hBN. For high computational efficiency, water molecules were represented by a simple point-charge SPC/E model with polarization correction.[46] The PBA-BODIPY molecule was built considering its protonation state at neutral pH, which involves the protonation of the amine terminus and leads to an overall total charge of +1 for the molecule. Two independent predictive tools, the pKa calculator of Marvin (version 23.5.0, 2023, Chemaxon: https://www.chemaxon.com), and the graph-based tool MolGpka,[47] were used to determine the protonated states of PBA-BODIPY amine terminus under neutral pH conditions. The PBA-BODIPY atomic partial charges were obtained from ATB by splitting the molecule into two parts and assigning the NH moiety as junction point. For Rbb, we modeled its zwitterionic form, which predominantly exists under neutral pH conditions as per the exfoliation experiment. Similar to PBA-BODIPY, the force field parameters of Rbb were obtained from ATB.[48-50] The atomic partial charges for Rbb were assigned based on values reported in the literature. Notably, the carboxylate group carries the negative charge, while the positive charge is distributed across the xanthenyl group, providing a dipolar moment that orients the phenyl ring perpendicular to the xanthenyl ring system.

For molecular dynamics (MD) simulations, non-bonded parameters were refined against experimental solvation properties; bonded parameters were assigned from existing force constants with a set of rules based on atom types and geometry. The geometric combining rule in Lennard-Jones (LJ) potential was employed for non–bonded interactions. The smooth particle-mesh Ewald (SPME) method was used to calculate the long-rang electrostatic interactions with a cutoff of 1.2 nm.[51] The simulations were performed with NPT ensemble and periodical boundary conditions in all directions, under constant pressure of P = 1 atm and constant temperature of T = 300 K. The simulation box had an initial height of 8 nm. The graphene and hBN sheet models had dimensions of 6.1 nm × 6.4 nm and 6.0 nm × 6.1 nm, respectively. The time step was set at 2 fs. After 50 ns initial equilibrium of a solvated 2D material (graphene/hBN) system, a dye molecule (PBA-BODIPY/Rbb) was introduced into the box by replacing some of the overlapping water molecules. The initial center-of-mass (COM) distance between the dye molecule and the nanosheet was set to be 2 nm; the dye, initially fixed in position, was released after 10 ns of re-equilibration, and its interaction with the system was monitored. Progress in dye adsorption was tracked by a stepwise addition of subsequent dye molecules onto a layer of already adsorbed surfactants until the maximum loading observed in the experiments has been reached. In each step, a new "free" dye molecule was placed 2 nm above the graphene/hBN basal plane. Then, the simulation was allowed to proceed until its adsorption was observed and stabilized.

2.4 Binding free energies calculations

Binding free energy (ΔG_{bind}) was calculated to help understand the dye adsorption process on the nanosheets in solution. For Rbb, ΔG_{bind} was predicted by an energy perturbation (FEP) approach, in line with our existing protocol,[28,40] while for PBA-BODIPY they were computed from the potential of mean force (PMF) obtained with umbrella sampling (US) simulations restrained along the distance between one dye molecule and the sheet (or two dye molecules if in solution).[52,53] Indeed, FEP calculations present inherent difficulties when applied to molecules presenting a net charge.[54] In principle, the non-physical gradual removal of the ligand could be coupled to a gradual removal of a distant counterion. However, due to the lack of *a priori* knowledge of the possible roles of counterions in the process, we decided to discard this

approach for PBA-BODIPY. We employed the weighted histogram analysis method (WHAM)[55-57] for post-processing the information from US simulations to construct the PMF, as implemented in GROMACS (version 2022.4) tools.[58-64] The PMF curves were calculated until a free-energy plateau was observed using distances ranging from 0.3 to 2.4 nm. The distance resolution and force constants for the simulated windows were first set to 0.02 nm and 5000 $kJ \cdot mol^{-1} \cdot nm^{-2}$. The resolution value was then refined to 0.01 nm in the regions 0.4-0.7 nm and 0.8-0.9 nm. The force constant was also adjusted in an *ad-hoc* fashion for sampling these less accessible regions. Thus, force constants of 7500, 10000, 12500 $kJ \cdot mol^{-1} \cdot nm^{-2}$ were adopted to assure a satisfactory degree of histogram overlap. ΔG_{bind} was then obtained by the difference between the free-energy plateau of the PMF curve and its minimum value.

For the FEP calculations, we evaluated the binding free energy as:

$$\Delta G_{bind} = \Delta\Delta G = \Delta G_{decoup} - \Delta G_{solv}$$

where ΔG_{decoup} and ΔG_{solv} are the decoupling free energy of an adsorbed surfactant molecule over graphene or hBN, and the solvation free energy of a surfactant molecule in water, respectively. To initiate the FEP calculations, we utilized the equilibrated configurations extracted from MD simulations, ensuring a reliable foundation for our FEP analysis. A time step of 1 fs and a total of 25 intermediate states were used, aligned with previous studies.[40] Each intermediate state was sampled for a duration of 4 ns. The multistate Bennett acceptance ratio (MBAR) method was employed to compute the change in free energy associated with the annihilation process, using the open-source alchemical analysis script.[53]

3. Results and discussion

3.1 LPE of graphite and bulk hBN

Rbb and PBA-BODIPY dyes have been investigated as dispersants for assisted-LPE of graphite and bulk hBN. The structures of Rbb and PBA-BODIPY derivative are shown in **Figure 1a**. The exfoliation process is shown as a flowchart in **Figure S1**. The exfoliated G-Rbb and G-BODIPY were prepared by bath sonication and collected by centrifugation. The exfoliated hBN-Rbb with pink color and hBN-BODIPY with orange color were prepared first by ball milling to get homogeneous powders, followed by bath sonication and centrifugation. The

excess of dispersants was removed by filtration, and the exfoliated nanosheets were then sonicated and re-dispersed in water. The yields of the resulting G-Rbb, hBN-Rbb, G-BODIPY and hBN-BODIPY dispersions were 1.9%, 5.0%, 1.9% and 6.2%, respectively. The exfoliation of hBN with Rbb and PBA-BODIPY showed higher efficiency in comparison with previous publications concerning aqueous phase productions, such as those using sodium pyrene-1-sulfonate (**Table S1**). As can be observed in **Figure 1b**, the exfoliated graphene and hBN sheets were well-dispersed in aqueous phase at a concentration of 0.2 mg/mL. The zeta potential values of graphene and hBN dispersions exfoliated with Rbb and PBA-BODIPY were found to be around -30 mV, indicating a good colloid stability.[65]

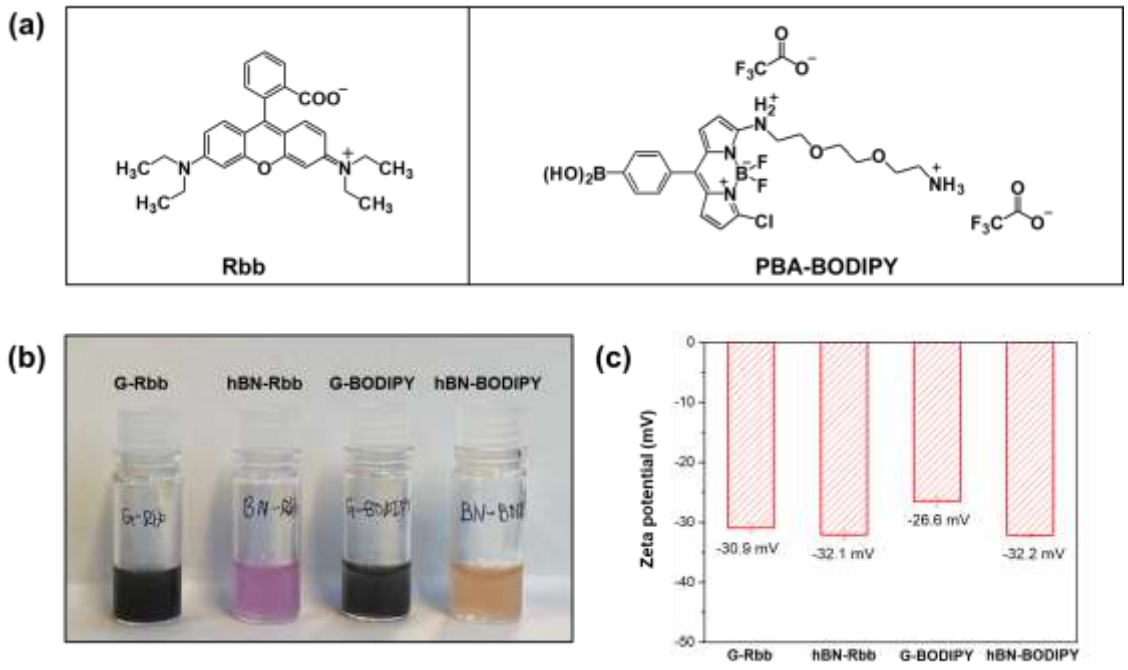

Figure 1. (a) Chemical structure of Rbb and PBA-BODIPY. (b) Digital photos of G-Rbb, hBN-Rbb, G-BODIPY and hBN-BODIPY suspended in water at a concentration of 0.2 mg/mL. (c) Zeta potential of G-Rbb, hBN-Rbb, G-BODIPY and hBN-BODIPY.

In order to investigate the dispersion and size distribution of the exfoliated sheets in aqueous solution, a small quantity of each dispersion was deposited on a TEM grid (**Figure 2**). These observations were complemented by statistics based on TEM images, permitting also to verify the sheet size (**Figure 2**). In the set of G-Rbb, graphite was exfoliated to few- and multi-layer sheets. In the TEM images we also observed some folded graphene nanosheets (**Figure 2a**).

Most of the graphene sheets exfoliated with rhodamine had a lateral size around 200 to 600 nm (with the average centered at 465 nm) (**Figure 2b**). In the case of hBN-Rbb (**Figure 2c**), the lateral size was smaller with a range of 100 nm to 300 nm (with the average centered at 220 nm) (**Figure 2d**). The TEM images of G-BODIPY and hBN-BODIPY (**Figure 2e** and **g**) revealed that the exfoliated nanosheets were produced with a larger lateral size distribution from 50 nm to 2000 nm (**Figure 2f** and **h**). Among them, G-BODIPY and hBN-BODIPY with a size below 600 nm were 68.1% and 69.5%, respectively.

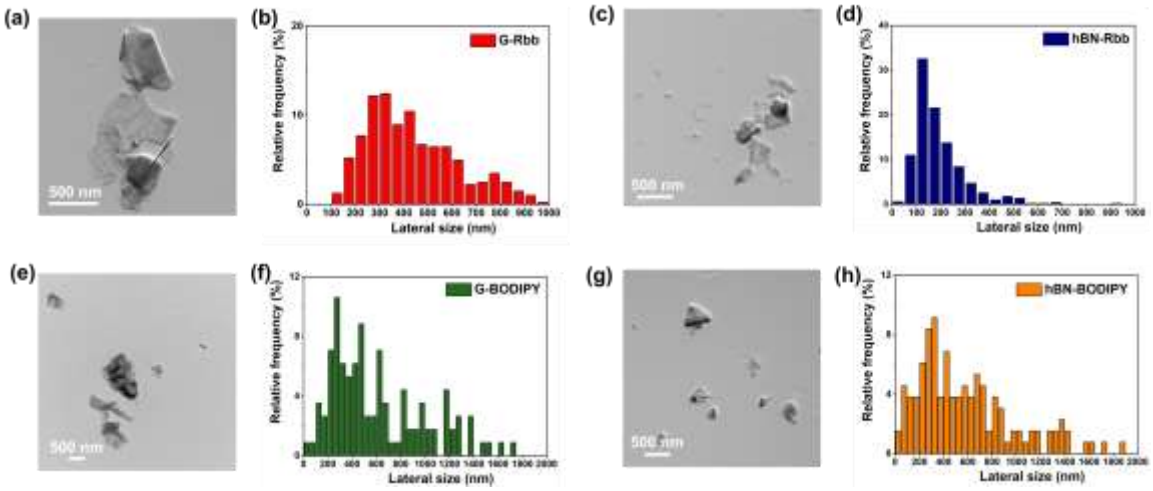

Figure 2. TEM images and histograms of lateral size distribution obtained by TEM analysis of (a,b) G-Rbb sheets, (c,d) hBN-Rbb, (e,f) G-BODIPY and (g,h) hBN-BODIPY.

High-resolution (HR) TEM was then used to determine the number of layers in the different exfoliated nanosheet samples. **Figure 3** shows the representative HRTEM images of exfoliated graphene and hBN. G-Rbb and hBN-Rbb appear as transparent film-like structures. According to the counted number of layers, G-Rbb comprised few-layered (2-5 layers) and multi-layered sheets (6-10 layers) with a proportion of 44.3% and 35.2%, respectively. For hBN-Rbb, the amount of few-layers and multi-layers was 47.3% and 33.2%, respectively. The electron diffraction pattern of the exfoliated sheets exhibited the six-fold symmetry nature of carbon atoms in graphene plane and hBN, indicating that a good crystallinity is maintained after the exfoliation (**Figure S2**). In the HRTEM images of G-BODIPY and hBN-BODIPY, we observed some curled edges and multi-layered nanosheets, revealing that these two materials contained also small amounts of thicker layers. The percentages of few-layered sheets and multi-layered

sheets in G-BODIPY were 41.2% and 25.6%, respectively, while in hBN-BODIPY they were 46.0% and 33.7%. Overall, the average number of layers for G-Rbb, hBN-Rbb, G-BODIPY and hBN-BODIPY was 8, 7, 10 and 8, respectively. Besides, AFM was performed to analyze the thickness of the exfoliated sheets. The height profile from local AFM analysis revealed varying thickness, likely resulting from the overlapping of various sheets. From the height of each terrace, the thickness of G-BODIPY sheets can be evaluated to be mostly between 4 and 8 nm (**Figure S3)**. Similar is the distribution observed for G-Rbb, which measured thickness ranged from 4 to 18 nm (**Figure S4**). Regarding the AFM thickness profile of hBN-BODIPY, these showed sheets with a thickness ranging from 2 to 25 nm, with most of the sheets having a height below 10 nm (**Figure S5**). Likewise, the thickness of hBN-Rbb ranges from 2 to 50 nm, with a distribution indicating that the majority of sheets are below 15 nm (**Figure S6**). Based on our previous experience with graphene and boron nitride exfoliation, these measurements correspond to the production of few-layer graphene and hBN, with particles composed, in average, of less than 10 layers.[28,35]

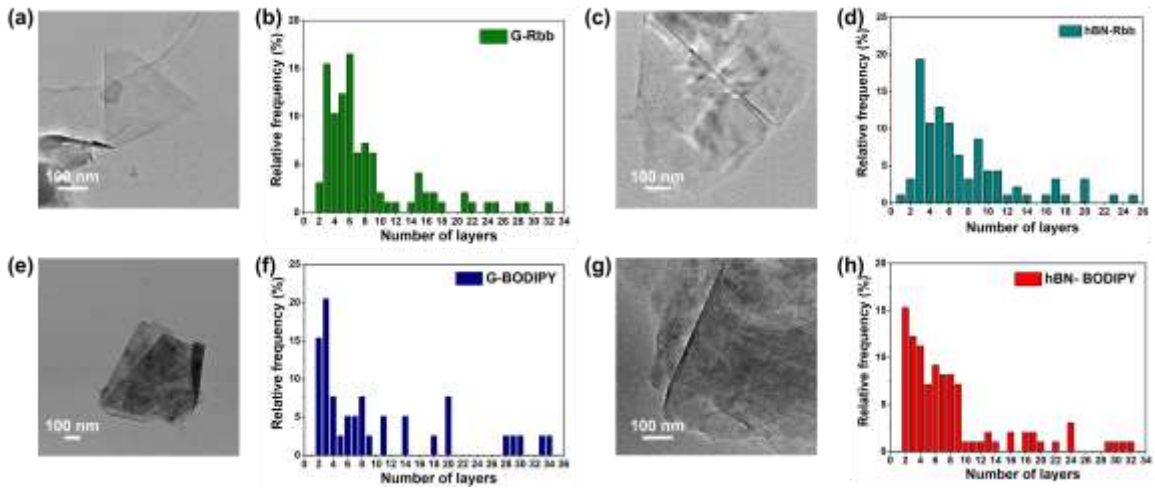

Figure 3. Representative high-resolution TEM images and histograms representing the number of layers of (a,b) G-Rbb sheets, (c,d) hBN-Rbb, (e,f) G-BODIPY and (g,h) hBN-BODIPY.

Subsequently, the Raman spectra of G-Rbb, hBN-Rbb and G-BODIPY were recorded to confirm the good quality and low defect content of the exfoliated sheets. The Raman spectra of G-Rbb and G-BODIPY showed three typical bands, corresponding to the D band around 1350 cm^{-1}, the G band around 1575 cm^{-1} and 2D band around 2695 cm^{-1} (**Figure S7a** and **S7c**). The

I_D/I_G ratio value was used to estimate the number of defects in graphene. The I_D/I_G ratio values of G-Rbb and G-BODIPY were 0.32 and 0.18, respectively, which were comparable with previous publications, implying low amount of defects.[66,67] Moreover, the value of I_{2D}/I_G ratio can be used to determine the number of graphene layers.[68] G-Rbb and G-BODIPY, with an I_{2D}/I_G ratio of 0.62 and 0.45, respectively, were considered few-layers (less than 5) and multi-layers (5-10 layers). The higher I_{2D}/I_G ratio of G-Rbb suggested a lower number of layers, which was consistent with the number of layers measured by HRTEM, showing 44.3% few-layer content.[69] The single band in hBN-Rbb at 1366.1 cm^{-1} is ascribed to the E_{2g} phonon vibration mode, with a full width at half-maximum (FWHM) corresponding to 9.6 cm^{-1} similar to the value reported in the literature (**Figure S7b**).[70] The red shifted E_{2g} band as well as the increase of FWHM compared with the reported bulk hBN of 4.77 cm^{-1} demonstrated the effective decreased thickness after exfoliation.[71] Besides, due to the high loading and tight attachment of PBA-BODIPY onto the hBN surface, the Raman spectrum of hBN-BODIPY exhibited a very strong fluorescence originating from the dye, resulting in the obscuring of the hBN band (**Figure S7d**).

The Rbb and PBA-BODIPY loading percentages on the nanosheets were determined by TGA (**Figure S8**). The weight percentages of Rbb loading for G-Rbb and hBN-Rbb were 7.6 and 9.5 wt%, respectively, while PBA-BODIPY weight loading percentages for G-BODIPY and hBN-BODIPY corresponded to 30.1 and 24.7 wt%, respectively. It is noteworthy that the PBA-BODIPY weight loading was much higher compared with the Rbb weight loading. This high loading of PBA-BODIPY compared to Rbb and other reported dispersants, such as 16% flavin mononucleotide on hBN, led to a higher exfoliation yield.[40]

The exfoliated graphene and hBN sheets were further characterized by XPS. The survey spectra and high-resolution spectra are shown in **Figure S9** and **S10**. The atom percentages are summarized in **Table S2**. The presence of F and Cl in the spectra of G-BODIPY and hBN-BODIPY correspond to the adsorbed PBA-BODIPY moiety. The increased amount of oxygen in G-Rbb and BN-Rbb is due to the Rbb moiety. The high-resolution spectra were also analyzed, confirming the presence of PBA-BODIPY and Rbb on both materials (see Supporting Information for a more detailed discussion of the XPS data). Besides, the XRD of graphite, bulk hBN and exfoliated nanosheets have been performed. As shown in the **Figure S11**, the peaks

of the exfoliated materials align with those of bulk graphite and hBN, but with decreased peak intensity. This suggests that the produced sheets have a good crystalline structure.

The stability of exfoliated materials was investigated using UV-Vis spectroscopy (**Figure S12**). The G-Rbb, hBN-Rbb, G-BODIPY and hBN-BODIPY at a concentration of 0.2 mg/mL were kept over 24 h at room temperature. The dispersions were analyzed by UV-Vis spectroscopy at different time points (2, 4, 6 and 8 h). After 24 h, the dispersions were sonicated for 3 min and observed again by UV-Vis spectroscopy. Overall, all the materials can be redispersed after bath sonication, demonstrating good stability. Additionally, we observed that the dyes remained stable on the nanosheets, with nearly no released dye in the supernatant even after 7 days (Figure S13).

The dispersions of the exfoliated materials were then investigated by UV-Vis spectroscopy (**Figure 4a** and **4b**). The maximum absorbance of PBA-BODIPY was observed at around 460 nm, but we could not see this peak in the spectra of G-BODIPY and hBN-BODIPY, likely due to the tight adsorption of the exfoliating molecule onto the surface of graphene and hBN (**Figure 4a)**. This observation was in good agreement with the values of the binding free energy (*vide infra*). Oppositely, the maximum absorbance of Rbb was red-shifted from 555 nm to 587 nm and 563 nm (**Figure 4b)**, confirming the interaction of this dye with the nanosheets. Compared to the spectrum of Rbb alone, the absorbance related to Rbb was very low due to the strong interaction of the dye with the materials. We investigated further the photoemission properties of G-BODIPY and hBN-BODIPY, measuring the fluorescence emission after excitation at 460 nm. The spectra of G-BODIPY and hBN-BODIPY exhibited a very small peak attributed to PBA-BODIPY located at 533 nm and 538 nm, respectively, characterized by a blue shift compared to free PBA-BODIPY at 542 nm (**Figure 4c**). The emission spectra of Rbb, G-Rbb and hBN-Rbb were recorded under 560 nm excitation wavelength. The emission peak was located at 575 nm and no shift of this peak was observed in this case in the spectra of G-Rbb and hBN-Rbb. The intensity of PBA-BODIPY and Rbb peaks on the exfoliated graphene was very low compared to hBN, indicating a higher fluorescence quenching capacity of graphene.

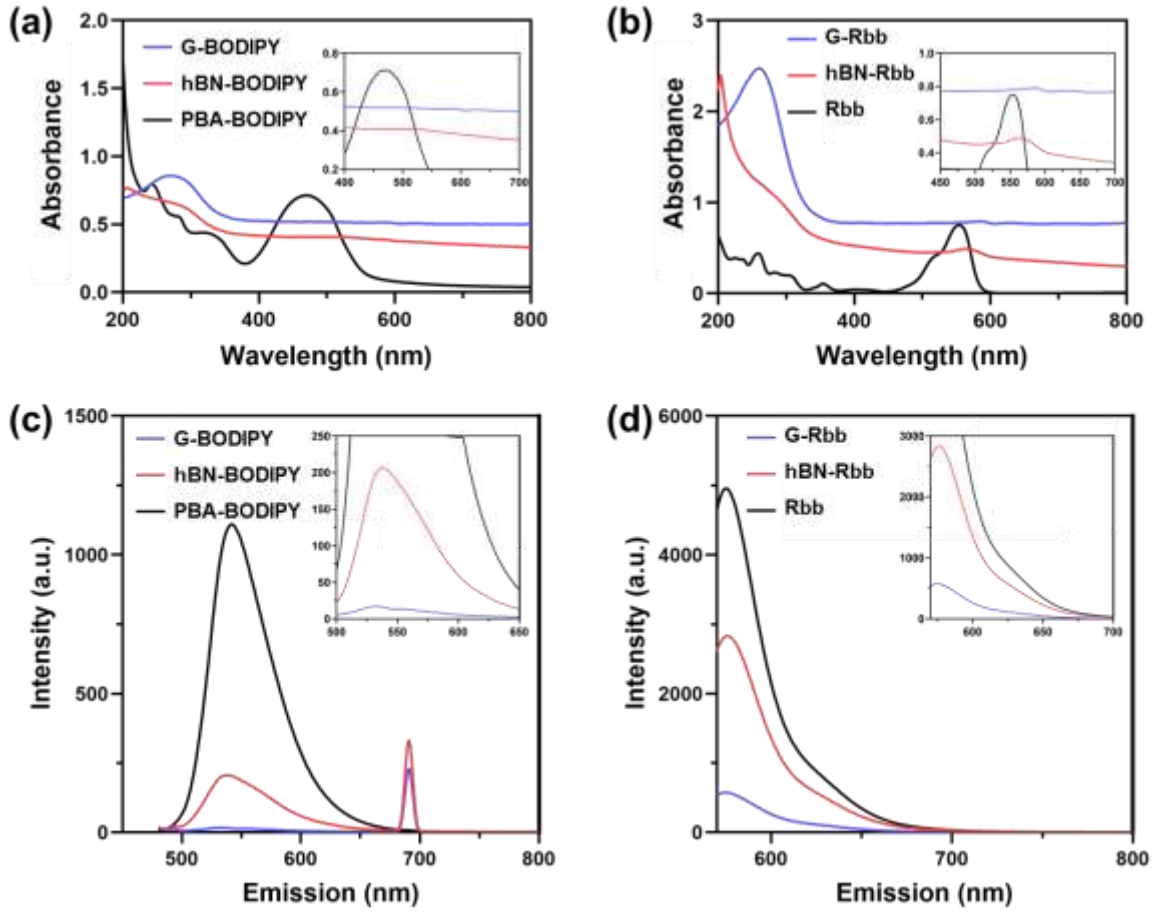

Figure 4. UV-Vis spectra of (a) PBA-BODIPY (50 µg/mL), G-BODIPY and hBN-BODIPY, (b) Rbb (2 µg/mL), G-Rbb and hBN-Rbb. Fluorescence emission spectra of (c) PBA-BODIPY, G-BODIPY and hBN-BODIPY under excitation at 460 nm, (d) Rbb, G-Rbb and hBN-Rbb under excitation at 560 nm. The concentration of G-BODIPY, hBN-BODIPY, G-Rbb and hBN-Rbb were all 100 µg/mL.

3.2 Molecular insights into PBA-BODIPY and Rbb adsorption onto graphene and hBN layers

A pivotal element in the success of LPE is the spontaneous adsorption of dye molecules onto the hBN/graphene basal plane. Understanding the role of dyes in enhancing LPE efficiency necessitates a detailed molecular analysis of their adsorption behavior on the basal plane of each 2D material. To this end, we incorporated MD simulations, which offer insights at a resolution not typically accessible through experimental methods.

The primary objective of our MD simulations was to provide a molecular-level understanding

of dye-2D material interactions. To this end, we chose to focus on the most fundament question, i.e. how dye molecules adsorb to the basal plane of a nanosheet, and calculate the adsorption free energy of this interaction. Spontaneous adsorption of dye molecules on the basal plane is a basic requirement for successful LPE, as it plays a crucial role in preventing re-aggregation of nanosheets after LPE. In other words, dye molecules that cannot adhere spontaneously to the basal plane do not contribute to the LPE process. For the systems under consideration, we prove this process is energetically favorable, and our free-energy calculations showed an affinity trend that nicely correlates with the adsorption yield observed in the experiments. Our objective was twofold: i) to determine the affinity of PBA-BODIPY and Rbb dye towards the graphene and hBN surfaces, thereby elucidating the molecular interactions that govern the adsorption phenomena on the basal plane; and ii) to investigate potential molecular patterns that arise from the self-assembly of the adsorbed dyes on these nanosheets.

To reach these goals, we performed successive MD simulations to model a stepwise addition of one adsorbate molecule on top of the nanosheet (see Experimental section 2.3). In other words, the migration of the dye molecules from the bulk water phase to an aqueous hBN or graphene sheet was evaluated at different degrees of surface coverage. Our focus initiates with the initial interaction between the fluorophores and 2D materials, establishing the foundation for subsequent self-assembly behaviors. Both fluorophores demonstrate spontaneous adsorption onto the basal plane of both graphene and hBN (**Movies S1-S4**). Following the stabilization of the first adsorbed fluorophore, more fluorophores were sequentially introduced into the solvent phase, leading to its spontaneous adsorption onto the basal plane of the 2D material and self-assembly with the already adsorbed fluorophores (**Figure S14**). Notably, PBA-BODIPY exhibits faster and more stable adsorption kinetics compared to Rbb, forming a single-layer close-packed self-assembly. In contrast, Rbb manifests non-uniform stacking on graphene and a close-packed self-assembly on hBN. Next, we started to simulate the interactions of PBA-BODIPY with graphene and hBN. We considered up to N=10 and 8 PBA-BODIPY molecules on graphene and hBN, respectively, based on the values calculated by the thermogravimetric analysis and on the periodicity of the simulation box (**Figure 5** and **Figure S15** and **S16**).

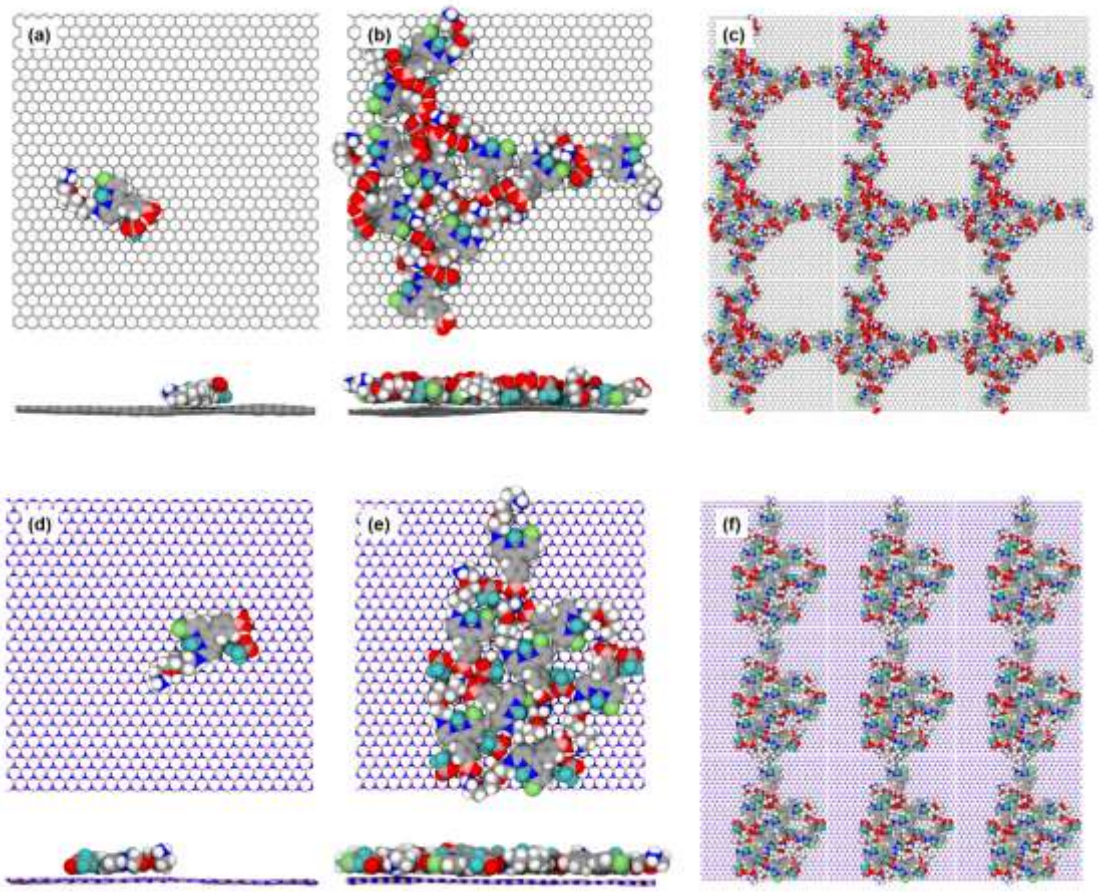

Figure 5. MD simulation snapshots of the adsorption and assembly formed by PBA-BODIPY on graphene (a-c) and hBN (d-f). Panels (c) and (f) show the periodic duplicate at the maximum load. Color legend: C, grey; B, pink; N, blue; O, red; Cl, lime green; F, forest green; H, white. Water is not shown for clarity.

The adsorption of a single PBA-BODIPY molecule on graphene was mainly driven by π-π interactions between the graphene basal plane and the PBA-BODIPY core through direct pairing. The single adsorbate molecule presented a coiled conformation due to favorable intramolecular interactions (**Figure 5a**). The addition of a second molecule led to the formation of a dimer of coiled molecules, assisted by the interactions between the NH_3^+ and $B(OH)_2$ moieties (**Figure S15**). Further introduction of the dispersant evidenced the formation of a molecular aggregate, which tends to spread out on the sheet. In addition, it was possible to spot the emergence of a reticular assembly pattern of PBA-BODIPY molecules when observing the periodic images of the simulation box (**Figure 5b** and **5c**). Of interest, the TFA (trifluoroacetic

acid) counterions could adsorb via the F atoms exposing both O of the carboxylate moieties to the medium, allowing for the occurrence of H-bond networks (**Figure S17** and **S18**). The growth of the molecular aggregate occurred through the direct binding of a new PBA-BODIPY molecule to the already adsorbed dyes. This self-assembly mechanism is in line with the gain in the free energy of binding observed at N ≥ 2 (i.e. N=number of exfoliating molecules) values (*vide infra*).

At low coverage, the adsorption on hBN resembled that on graphene (**Figures 5d-5f** and **Figure S16**), being governed by the stacking of the PBA-BODIPY core. Dimer formation was assisted by the presence of adsorbed counterions (see **Figure 5e**). Noteworthy is the fact that, at higher concentrations, the dyes are less spread out on the hBN sheet when compared to graphene, which implicates no long-range ordering (compare **Figure 5c** and **5f**). Moreover, there is also a different behavior of the counterions, which adsorb now in a parallel orientation to the hBN surface.

Interestingly, the adsorption of Rbb molecules on graphene and hBN exhibits a stark difference to PBA-BODIPY. A single Rbb molecule adsorption onto graphene was initiated by the hydrophobic interaction between the nitrogen-containing diethylamino group and the surface of graphene, then stabilized by π–π stacking between the plane moiety (the xanthene group) of Rbb and graphene. The equilibrated single Rbb molecule was nearly parallel to the graphene basal plane (**Figure 6a**). The polar moieties of Rbb, namely, the rotatable carboxylate group, remained clear from graphene, interacting with the surrounding water molecules. Upon adding a second Rbb molecule, it resulted in the formation of a dimer with a "3D conformation", where the planar group of one Rbb molecule stacking slightly tilted on another Rbb molecule which is parallel stacked onto graphene, leading to a more complex and less orderly arrangement of molecule assembly compared to the tile-assembled monolayer of Rbb (as seen on hBN). We noticed the formation of π–π stacking between the aromatic groups of the two Rbb molecules. Such 3D structure appeared to be stable at least within the simulated timescale (~100 ns). Based on the TGA results, we estimated that a simulated graphene can host up to 4 Rbb molecules. Further addition of Rbb molecules in MD simulation led to the formation of a bigger molecular assembly of Rbb, with stable 3D assembly (**Figure 6b**).

In the case of hBN, the adsorption of a single Rbb was spontaneous and predominately driven

by hydrophobic interaction between the aromatic moiety of Rbb and hBN basal plane. Notably, an equilibrated Rbb xanthene group resulted parallel to the basal plane of hBN, similar to the case on graphene (**Figure 6d**). However, we need to point out that the dipolar nature of the B-N bonds contributes to the relatively stronger interactions between Rbb and hBN compared to graphene. Introducing a second Rbb into the simulated system, we observed the spontaneous adsorption, followed by the formation of Rbb dimer superlattice on hBN (**Figure S19** and **S20**). We estimated that a simulated hBN can also host up to 4 of Rbb molecules based on the TGA. Further added Rbb would adsorb spontaneously, but would not disrupt the exhibiting dimers on hBN, as observed in the simulation snapshot with 4 Rbbs (**Figure 6e**). Four Rbb molecules self-assemble into two molecular islands consisting of a superlattice and an amorphous assembly, where a 3D structure is evident. Although no H-bonds were found between the dimer molecules, we noticed the resemblance to another system we previously studied, where pairs of adsorbed flavin mononucleotide molecules on hBN could form bidental H-bonds to stabilize their molecular assembly.[53] Free energy calculation confirmed that the main driving force of bidental superlattice formation were the electrostatic interactions between the diethylamino groups of two Rbb molecules.

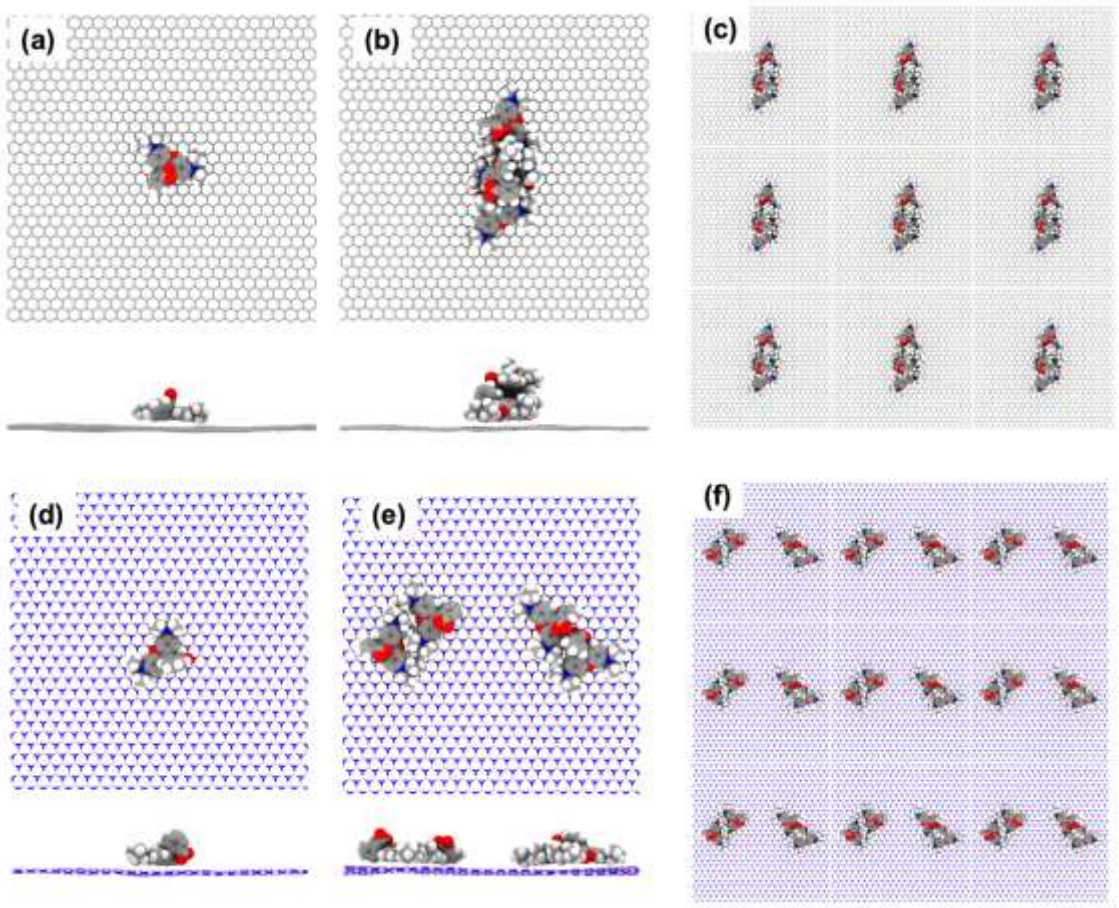

Figure 6. MD simulation snapshots depicting the adsorption and assembly formed by Rbb on graphene (a-c) and hBN (d-f). Panels (c) and (f) showcase the periodic duplicate at the maximum load. The color legend denotes carbon (C) in grey, boron (B) in pink, nitrogen (N) in blue, oxygen (O) in red, and hydrogen (H) in white. Water molecules are omitted for clarity.

The calculated binding free energies (ΔG_{bind}) are shown in **Table 1**. The negative values confirmed that the adsorption of both dyes is always thermodynamically favored (e.g., occurring spontaneously) and dominates significantly over the energy gained from the simple dye dimerization in solution (-47.1 kJ/mol for PBA-BODIPY and -28.3 kJ/mol for Rbb). Overall, it evidences a higher affinity of the dispersants for hBN over graphene. This is reflected by the lower ΔG_{bind} obtained for all systems involving the hBN material. This evidence correlates well with the experimental conclusions pointing to higher yields when producing the exfoliated hBN nanosheets.

Focusing now on the hBN material, as the coverage of either PBA-BODIPY and Rbb increases, the binding free energy decreases. In other words, for the coverage extents analyzed in this work, the adsorbed dyes molecules assist in binding additional surfactants onto the hBN nanosheet, which is an indication of a cooperative mechanism of interaction. At the maximum loading scenario, the incorporation of an additional dye molecule is much more preferred than the single dye molecule attaching to the nanosheet, with PBA-BODIPY outperforming Rbb.

At the contrary, when the graphene nanosheet is considered, the interaction of a second dye molecule is still more favorable than the adsorption of the first dye molecule, but the results do not indicate a substantial free energy gain for further adsorption (N >2). For PBA-BODIPY, as suggested in another computational study on a related topic,[76] the interplay between a higher interaction energy (e.g., -365.2 and -166.4 kJ/mol for hBN and graphene, respectively, considering the single adsorption) and entropic changes (on both adsorbates and solvent)[77,78] might explain the lower ΔG_{bind} values for hBN nanosheets. In addition, PBA-BODIPY tends to form aggregates that increase in size as the number of molecules N increases.

The limited cooperativity effect observed for its adsorption on graphene might be entropy driven. Desorption of one molecule involves the increase of the conformational freedom of both the solvated molecule and the adsorbed aggregate. At the highest loading (N=10), this contribution might overcome any energetic gains related to further adsorption. In the case of Rbb, the assistance of adsorbed molecules is also limited. Rbb exhibits a unique assembly pattern on graphene, forming stacks of dye that are not limited to a single layer but can also be intercalated on top or adopt a "3D" conformation, which has a smaller binding energy (-80.3 kJ/mol for the Rbb in tilted adsorption conformation, compared to the parallel adsorbed Rbb on graphene), and which could explain the limited energy gain for graphene at increasing loading. These different assembly characteristics contribute to the different adsorption behavior and intermolecular interactions between the dispersants and the 2D materials.

Table 1. Free energy of binding ΔG_{bind} (kJ/mol) calculated from detaching one molecule of PBA-BODIPY (or Rbb) from graphene/hBN interfaces with N dye molecules adsorbed.

	graphene			**hBN**		
N (PBA-BODIPY)	**1**	**2**	**10**	**1**	**2**	**8**
	-96.6	-157.4	-154.7	-165.8	-186.7	-259.7
N (Rbb)	**1**	**2**	**4**	**1**	**2**	**4**
	-102.9	-108.6	-109.9	-170.0	-189.6	-205.1

4. Conclusion

In this work, we have demonstrated a simple and environmental-friendly way to exfoliate graphite and bulk hBN using bath sonication with the assistance of two aromatic dyes, and we provide a molecular understanding of the dyes' adsorption process that underpins layer exfoliation and solution stability. The two fluorescent dyes, Rbb and PBA-BODIPY, employed in this work possess unique properties and suitable structures for interaction with flat materials. With aromatic groups and hydrophilic moieties, they were found to be efficient exfoliating agents, and the resulting layered materials showed good dispersibility. This characteristic would be fundamental for the future development of novel fluorescent exfoliating compounds. The characterization by HRTEM and TGA demonstrated that few-layered and multi-layered sheets with a high dye loading were produced, while Raman spectroscopy confirmed that the quality of the flakes was not affected during the exfoliation process. MD simulations offered valuable atomistic and energetic insights into the mechanisms governing the spontaneous dispersant adsorption and self-assembly on the exfoliated basal plane of the studied 2D materials. Our findings revealed a pronounced affinity between the dispersants and 2D materials, coupled with a notable energetic gain resulting from increased dispersant coverage over the basal plane. As a result, a layer of the dye molecules forms on the exfoliated graphene and hBN with different patterns. These evidences underscore the significance of intermolecular interactions in achieving an effective surface coverage. Altogether, our comprehensive investigation provides crucial insights for the rational design and utilization of aromatic dispersants in advancing the applications of 2D materials in the domains of materials science and biomedicine.

Supporting Information

Supporting Information is available from the Wiley Online Library or from the author.

5. Acknowledgments

We gratefully acknowledge the financial support from PHC Merlion Program 2023 (Project 49627WG). This work was also supported by the Centre National de la Recherche Scientifique (CNRS), by the Agence Nationale de la Recherche (ANR) through the LabEx project Chemistry of Complex Systems (ANR-10-LABX-0026_CSC) and by Jean-Marie Lehn Foundation. The authors wish to thank Cathy Royer from the "Plateforme Imagerie In Vitro de l'ITI Neurostra" CNRS UAR 3156, University of Strasbourg (Strasbourg, France) for TEM analysis, Dr. Dris Ihiawakrim from the Transmission Electron Microscopy Platform at the IPCMS (Strasbourg, France) for the HRTEM analyses. YH is indebted to the Chinese Scholarship Council for supporting his PhD internship. M. A. L. acknowledges the Generalitat Valenciana for a postdoctoral fellowship (CIAPOS/2021/255). The authors gratefully acknowledge the financial support from the EU Graphene Flagship project (no. 881603). GCQDS, CG and PP are grateful to the University of Trieste for financial support and to CINECA national computing center for computational resources through the ISCRA initiative. XQ and HG acknowledge support from the Singapore Ministry of Education (MOE) under T1 Award #RG138/20, and a start-up grant from Nanyang Technological University, Singapore and A*STAR, Singapore. Molecular dynamics simulations reported were performed on resources provided by the High Performance Computing Centre at Nanyang Technological University, Singapore, the National Supercomputing Centre, Singapore (http://www.nscc.sg), and National Supercomputing Center, Italy (https://www.hpc.cineca.it/). CMM and BR thank the Ministries of Europe and Foreign Affairs (MEAE) and of Higher Education and Research (MESR) for their support through the PHC GALILEE 2022 program (project number 47791TD & G22_121). The authors are indebted to Haijun Peng and Paolo Samorì for their help in XRD analyses.

Received: ((will be filled in by the editorial staff))

Revised: ((will be filled in by the editorial staff))

Published online: ((will be filled in by the editorial staff))

References

[1] C. Zhu, D. Du, Y. Lin, *2D Mater.* **2015**, *2*, 032004.

[2] P. Tao, S. Yao, F. Liu, B. Wang, F. Huang, M. Wang, *J. Mater. Chem. A* **2019**, *7*, 23512.

[3] S. Angizi, S. A. A. Alem, M. H. Azar, F. Shayeganfar, M. I. Manning, A. Hatamie, A. Pakdel, A. Simch, *Prog. Mater. Sci.*, **2022**, *124*, 100884.

[4] S. Yu, X. Wang, H. Pang, R. Zhang, W. Song, D. Fu, T. Hayat, X. Wang, *Chem. Eng. J.* **2018**, *333*, 343.

[5] K. Hantanasirisakul, Y. Gogotsi, *Adv. Mater.* **2018**, *30*, 1804779.

[6] F. Shahzad, A. Iqbal, H. Kim, C. M. Koo, *Adv. Mater.* **2020**, *32*, 2002159.

[7] M. Chhowalla, Z. Liu, H. Zhang, *Chem. Soc. Rev.* **2015**, *44*, 2584.

[8] J. Ping, Z. Fan, M. Sindoro, Y. Ying, H. Zhang, *Adv. Funct. Mater.* **2017**, *27*, 1605817.

[9] L. Qina, S. Jiang, H. He, G. Ling, P. Zhang, *J. Control. Release.* **2020**, *318*, 50.

[10] V. Eswaraiah, Q. Zeng, Y. Long, Z. Liu, *Small* **2016**, *12*, 3480.

[11] S. M. Kim, A. Hsu, M. H. Park, S. H. Chae, S. J. Yun, J. S. Lee, D. H. Cho, W. Fang, C. Lee, T. Palacios, M. Dresselhaus, K. K. Kim, Y. H. Lee, J. Kong, *Nat. Commun.* **2015**, *6*, 8662.

[12] N. Wang, G. Yang, H. Wang, C. Yan, R. Sun, C. P. Wong, *Mater. Today* **2019**, *27*, 33.

[13] W. Luo, Y. Wang, E. Hitz, Y. Lin, B. Yang, L. Hu, *Adv. Funct. Mater.* **2017**, *27*, 1701450.

[14] A. Ciesielski, P. Samorì, *Adv. Mater.* **2016**, *28*, 6030.

[5] A. Ciesielski, P. Samorì, *Chem. Soc. Rev.* **2014**, *43*, 381.

[16] X. Zhang, A. C. Coleman, N. Katsonis, W. R. Browne, B. J. Wees, B. L. Feringa, *Chem. Commun.* **2010**, *46*, 7539.

[17] A. Jawaid, D. Nepal, K. Park, M. Jespersen, A. Qualley, P. Mirau, L. F. Drummy, R. A. Vaia, *Chem. Mater.* **2016**, *28*, 337.

[18] S. Roy, A. Mondal, V. Yadav, A. Sarkar, R. Banerjee, P. Sanpui, A. Jaiswal, *ACS Appl. Bio Mater.* **2019**, *2*, 2738.

[19] Z. Miao, D. Huang, Y. Wang, W. J. Li, L. Fan, J. Wang, Y. Ma, Q. Zhao, Z. Zha, *Adv. Funct. Mater.* **2020**, *30*, 2001593.

[20] X. Xu, J. Wu, Z. Meng, Y. Li, Q. Huang, Y. Qi, Y. Liu, D. Zhan, X. Y. Liu, *ACS Appl. Nano Mater.* **2018**, *1*, 5460.

[21] C. X. Hu, Y. Shin, O. Read, C. Casiraghi, *Nanoscale* **2021**, *13*, 460.

[22] R. J. Smith, P. J. King, M. Lotya, C. Wirtz, U. Khan, S. De, A. O'Neil, G. S. Duesberg, J. C. Grunlan, G. Moriarty, J. Chen, J. Wang, A. I. Minett, V. Nicolosi, J. N. Coleman, *Adv. Mater.* **2011**, *23*, 39448.

[23] D. Parviz, S. Das, H. S. T. Ahmed, F. Irin, S. Bhattacharia, M. J. Green, *ACS Nano*, **2012**,

6, 8857.

[24] H. Yan, Y. Hernandez, A. Schlierf, A. Felten, A. Eckmann, S. Johal, P. Louette, J.-J. Pireaux, X. Feng, K. Mullen, V. Palermo, C. Casiraghi, *Carbon* **2013**, *53*, 357.

[25] M. Lotya, Y. Hernandez, P. J. King, R. J. Smith, V. Nicolosi, L. S. Karlsson, F. M. Blighe, S. De, Z. Wang, I. T. McGovern, G. S. Duesberg, J. N. Coleman, *J. Am. Chem. Soc.* **2009**, *131*, 3611.

[26] S. De, P. J. King, M. Lotya, A. O'Neill, E. M. Doherty, Y. Hernandez, G. S. Duesberg, J. N. Coleman, *Small* **2010**,*6*, 458.

[27] X. Liu, G. Duan, W. Li, Z. Zhou, R. Zhou, *RSC Adv*. **2017**, *7*, 37873.

[28] M. A. Lucherelli, X. Qian, P. Weston, M. Eredia, W. Zhu, P. Samorì, H. Gao, A. Bianco, A. Bussche, *Adv. Mater.* **2021**, *33*, 2103137.

[29] M. Beija, C. A. M. Afonso, J. M. G. Martinho, *Chem. Soc. Rev.* **2009**, *38*, 2410.

[30] T. Zhang, C. Ma, T. Sun, Z. Xie, *Coord. Chem. Rev.* **2019**, *390*, 76.

[3] C. Liu, C. N. Scott, *Dyes Pigm.* **2021**, *196*, 109792.

[32] Y. SU, S. Lu, P. Ga, M. Zheng, Z. Xie, *Mater. Chem. Front.* **2019**, *3*, 1747.

[33] Y. Xue, J. Lee, H. J. Kim, H. J. Cho, X. Zhou, Y. Liu, P. Tebon, T. Hoffman, M. Qu, H. Ling, X. Jiang, Z. Li, S. Zhang, W. Sun, S. Ahadian, M. R. Dokmeci, K. J. Lee, A. Khademhosseini, *ACS Appl. Bio Mater.* **2020**, *3*, 6908.

[34] Z. Li, M. Zheng, X. Guan, Z. Xie, Y. Huang, X. Jing, *Nanoscale* **2014**, *6*, 5662.

[35] G. Reina, G. M. Beneventi, R. Kaur, G. Biagiotti, A. Cadranel, C. Ménard-Moyon, Y. Nishina, B. Richichi, D. M. Guldi, A. Bianco, *Chem. Eur. J*. **2023**, *29*, e202300266.

[36] S. Atilgan, Z. Ekmekci, A. L. Dogan, D. Gucb, E. U. Akkaya, *Chem. Commun.* **2006**, *42*, 4398.

[35] D. Maheshwaran, T. Nagendraraj, T. S. Balaji, G. Kumaresan, S. S. Kumaranc, R. Mayilmurugan, *Dalton Trans.* **2020**, *41*, 14680.

[35] T. Loret, L. A. V. De Luna, M. A. Lucherelli, A. Fordham, N. Lozano, A. Bianco, K. Kostarelos, C. Bussy, *Small* **2023**, *19*, 2301201.

[36] G. E. Giacomazzo, P. Palladino, C. Gellin, G. Salerno, V. Baldoneschi, A. Feis, S. Scarano , M. Minunni, B. Richichi, *RSC Adv.* **2019**, *9*, 30773.

[37] X. Qian, M. A. Lucherelli, C. Corcelle, A. Bianco, H. Gao, *Forces in Mechanics* **2022**, *8*, 100098.

[38] M. A. Creighton, W. Zhu, F. Krieken, R. A. Petteruti, H. Gao, R. H. Hurt, *ACS Nano* **2016**, *10*, 2268.

[39] A. K. Malde, L. Zuo, M. Breeze, M. Stroet, D. Poger, P. C. Nair, C. Oostenbrink, A. E.

Mark, *J. Chem. Theory Comput.* **2011**, *7*, 4026.
[40] S. Canzar, M. El-Kebir, R. Pool, K. Elbassioni, A. K. Malde, A. E. Mark, D. P. Geerke, L. Stougie, G. W. Klau, *J. Comput. Biol.* **2013**, *20*, 188.
[4] K. B. Koziara, M. Stroet, A. K. Malde, A. E. Mark, *J. Comput. Aided Mol. Des.* **2014**, *28*, 221.
[42] N. Schmid, A. P. Eichenberger, A. Choutko, S. Riniker, M. Winger, A. E. Mark, W. F. van Gunsteren, *Eur. Biophys. J.* **2011**, *40*, 843.
[43] H. J. C. Berendsen, J. R. Grigera, T. P. Straatsma, *J. Phys. Chem.* **1987**, *91*, 6269.
[44] X. Pan, H. Wang, C. Li, J. H. Zhang, C. Ji, *J. Chem. Inf. Model.* **2021**, *61*, 3159.
[45] W. Hehre, R. Ditchfield, J. Pople, *J. Chem. Phys.* **1972**, *56*, 32.
[46] F. London, *J. Phys. Radium* **1937**, *8*, 397.
[47] P. K. Walhout, Z. He, B. Dutagaci, G. Nawrocki, M. Feig, *J. Phys. Chem.* B **2022**, *126*, 10256.
[48] U. Essmann, L. Perera, M. L. Berkowitz, T. Darden, H. Lee, L. Pedersen, *J. Phys. Chem.* **1995**, *103*, 8577.
[49] J. Wang, Y. Deng, B. Roux, *Biophys. J.* **2006**, *91*, 2798.
[50] P. V. Klimovich, M. R. Shirts, D. L. Mobley, *J. Comput. Aided Mol. Des.* **2015**, *29*, 397.
[51] A. S. J. S. Mey, B. K. Allen, H. E. Bruce Macdonald, J. D. Chodera, D. F. Hahn, M. Kuhn, J. Michel, D. L. Mobley, L. N. Naden, S. Prasad, A. Rizzi, J. Scheen, M. R. Shirts, G. Tresadern, H. Xu, *Living J. Comput. Mol. Sci*. **2020**, *2*, 18378.
[52] A. M. Ferrenberg, R. H. Swendsen, *Phys. Rev. Lett.* **1989**, *63*, 1195.
[53] S. Kumar, D. Bouzida, R. H. Swendsen, P. A Kollman, J. P. Rosenberg, *J. Comput. Chem.* **1992**, *13*, 1011.
[54] B. Roux, *Comput. Phys. Commun.* **1995**, *91*, 275.
[55] M. Abraham, T. J. Murtola, R. Schulz, S. Páll, J. C. Smith, B. Hess, E. Lindahl, *SoftwareX* **2015**, *1*, 19.
[56] S. Páll, M. J. Abraham, C. Kutzner, B. Hess, E. Lindahl, *Lecture Notes in Computer Science*, Springer, Cham, **2015**.
[57] S. Pronk, S. Páll, R. Schulz, P. Larsson, P. Bjelkmar, R. Apostolov, M. R. Shirts, J. C. Smith, P. M. Kasson, D. Spoel, B. Hess, E. Lindahl, *Bioinformatics* **2013**, *29*, 845.
[58] B. Hess, C. Kutzner, D. Spoel, E. Lindahl, *J. Chem. Theory Comput.* **2008**, *4*, 435.
[59] D. V. D. Spoel, E. Lindahl, B. Hess, G. Groenhof, A. E.Mark, H. J. C. Berendsen, *J. Comput. Chem.* **2005**, *26*, 1701.
[60] E. Lindahl, B. Hess, D. V. D. Spoel, *J. Mol. Model.* **2001**, *7*, 306.

[61] H. J. C. Berendsen, D. V. D. Spoel, R.V. Drunen, *Comput. Phys. Commun.* **1995**, *91*, 43.

[62] W. Liu, C. Zhao, R. Zhou, D. Zhou, Z. Liu, X. Lu, *Nanoscale* **2015**, *7*, 9919.

[63]M. A. S. Badri, M. M. Salleh, N. F. M. Noor, M. Y. A. Rahman, A. A. Umar, *Mater. Chem. Phys.* **2017**, *193*, 212.

[64] S. R. Shin, D. S. Lee, *Nanomaterials* **2022**, *12*, 685.

[65] U. Kalsoom, M. S. Rafique, S. Shahzadi, K. Fatima, R. Shaheen, *Mater. Sci.-Pol.* **2017**, *35*, 687.

[66] Z. Lin, P. S. Karthik, M. Hada, T. Nishikawa, Y. Hayashi, *Nanomaterials* **2017**, *7*, 125.

[67] A. Chae1, S. J. Park, B. Min, I. In, *Mater. Res. Express* **2018**, *5*, 015036.

[68] N. Mittal, G. Kedawat, Kanika, S. Gupta, B. K. Gupta, *Chemistry Select* **2020**, *5*, 12564.

[69] H. Heinz, H. Ramezani-Dakhel, *Chem. Soc. Rev.* **2016**, *45*, 412.

[70] A. Striolo, B. P. Grady, *Langmuir* **2017**, *33*, 8099.

[71] T. K. Mukhopadhyay, A. Datta, *Phys. Chem. Chem. Phys.* **2020**, *22*, 22157.